# The Scattering of 31.5-Mev Protons from Several Elements[*,†]

Roy Britten[‡,§]

*Palmer Laboratory, Princeton University, Princeton, New Jersey*

(Received January 30, 1952)

The elastic and inelastic scattering of 31.5-Mev protons from the Berkeley linear accelerator from Be, C, Al, Pb, and Pt have been observed, using a sodium iodide (Tl) crystal and photomultiplier for particle detection and energy measurement. Inelastic scattering led to the excitation of states or closely spaced groups of states at 2.5, 6.8. and 11.6 Mev in beryllium; 4.3, (7.5), and 9.5 in carbon; and a group of states between 11 and 17 in carbon. Deuterons have been observed from the reaction $C^{12}(p, d)C^{11}$, leading to the ground state of $C^{11}$. Differential cross sections have been measured for all these reactions at two or three angles. The differential cross sections for the elastic scattering of 31.5-Mev protons have been measured at several angles for $Be^9$, $C^{12}$, $Al^{27}$, and Pb. A comparison with the results of calculations based on several different nuclear models is made. The extreme sensitivity of the calculated cross sections (in the backward hemisphere) to the individual phase shifts and amplitudes indicates that moderately rough measurements of the backward scattering cross sections of nuclei for neutrons in this energy range would give accurate determinations of the individual phase shifts.

## I. INTRODUCTION

ALTHOUGH a thorough understanding of the scattering of nucleons by nucleons may not be achieved for some time, information of importance to the development of concepts of nuclear structure may be obtained at present from the scattering of nucleons by complex nuclei. Such experiments supply two quite distinct kinds of information. From the inelastic scattering process information may be obtained about some of the excited states of the bombarded nucleus. From the angular distribution of the elastically scattered particles information may be derived about some aspects of the structure of the nucleus, or better, about the "external" characteristics of the nucleus that influence the colliding particle.

The present work is an exploration of the scattering of 31.5-Mev protons by means of the thallium-activated sodium iodide crystal photomultiplier[1] technique. With this technique it is possible to record on film the entire energy spectrum of outgoing particles at one time.

## II. APPARATUS AND METHOD

### A. The Linear Accelerator

The linear accelerator[2] produces a beam of approximately 32-Mev protons with an energy spread of about 0.6 Mev (full width at half-maximum). The proton current occurs in pulses of 150 to 200 microsecond

duration at a 15 cps repetition frequency. The energy produced and the energy spread depend critically on adjustments of the end drift tubes which affect the distribution of radio frequency power along the cavity. As a result, it is necessary to check the beam energy regularly. This was done for these experiments by measuring the range of the protons in aluminum, using a remote control foil changing device.

At the exit end of the accelerator a magnet deflects the beam. This magnet is principally used for switching the beam from one experimental set-up to another. In this work it was not practical to use the magnet to reduce the energy spread of the main group of protons. The magnet did, however, remove a small number of protons of intermediate energies and a group of 8-Mev protons. This group of 8-Mev protons results from the acceleration on alternate cycles of $H_2^+$ ions. These ions remain approximately in resonance and achieve an energy of about 16 Mev. A 16-Mev $H_2^+$ ion has the same momentum as a 32-Mev $H^+$ ion, and therefore a thin nylon foil is placed in the beam ahead of the magnet to convert the $H_2^+$ (16-Mev) ions to $H^+$ (8-Mev) ions.

The angular divergence of the proton beam is quite small ($\pm 0.1°$). The pre-magnet collimator $A$ (Fig. 1) was set to a $\frac{1}{8}$-in. square aperture and most of the proton current passed through a $\frac{3}{16}$-in. diameter circular aperture at $C$. Under these conditions, the principal spot of proton beam at the scattering foil $F$ was about $\frac{1}{4}$ in. in diameter. A 1-in. diameter collimator was placed at $G$ to prevent slit-scattered protons from striking the foil holder.

This arrangement gave only a small gamma-ray background for several reasons. The main part of the excess proton current was stopped at $A$ which was a long distance (10 ft) from the scattering chamber, with the magnet acting as shielding. A relatively small amount of current was stopped at $C$. The current density at the edges of aperture $C$ was much smaller than that at the center. Seven hundred pounds of lead

[1] Franzen, Peelle, and Sherr, Phys. Rev. **79**, 742 (1950).

[2] L. W. Alvarez, Phys. Rev. **70**, 799 (1946); Science **106**, 506 (1946); unpublished Manhattan District Declassified Contribution No. 85 (1946); unpublished Atomic Energy Commision Unclassified Report No. 120 (1948); unpublished University of California Radiation Laboratory Report No. 236 (1948).
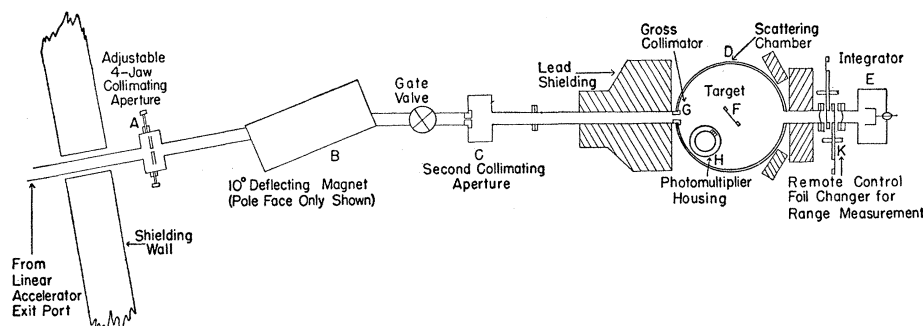
FIG. 1. Arrangement of scattering chamber in linear accelerator bombardment area.

shielding was placed around the scattering chamber as shown in Fig. 1.

In Fig. 3 is shown the resulting background taken with the scattering foil removed from the proton beam. Before the careful collimation and shielding was completed, the background was so great as to mask the deuteron peak, at channel 16, in the 90° carbon curve.

## B. The Scattering Chamber

A cross section of the scattering chamber at 90° to the beam direction is shown in Fig. 2. The main body of the chamber is a brass cylinder 19 in. in diameter with $\frac{1}{2}$-in. thick walls. This chamber carries the connections to the beam tube and integrator and is rigidly mounted to the table top.

The base plate which carries the photomultiplier housing and foil holder is a 19-in. diameter $1\frac{1}{4}$-in. thick iron plate. This plate is supported by three adjustable ball bearing wheels and is accurately centered by three guides attached to the supports for the brass cylinder. When the chamber is let down to atmospheric pressure, the weight of the base plate is carried by the ball bearing wheels, and it may easily be rotated for angle changes. When it is set at the desired angle, the foil angle is adjusted by laying a scale across the foil holder and setting it to one of several angle marks on the inside of the brass cylinder.

The controlling aperture for particles striking the crystal was a $\frac{1}{4}$-in. diameter hole located $4\frac{5}{8}$ in. from the center of the scattering chamber. This corresponds to a solid angle subtended of $2.29 \times 10^{-3}$ steradian. The proton beam struck the target principally within a circular region $\frac{1}{4}$-in. in diameter, which was centered over the center of the scattering chamber to an accuracy of about $\pm\frac{1}{8}$-in. As a result, the scattering angle for the center of the counter aperture could be set to an accuracy of $\pm1.5°$ and the angular resolution was about 6°.

The gross collimator (G) on Fig. 1 was intended to prevent slit-scattered protons from striking the foil holder. Tests were made at both 90° and 160° with the foil holder but no scattering foil in place. No counts were observed in excess of the usual $\gamma$-ray and neutron background.

## C. The Photomultiplier Assembly

A type 5819 photomultiplier was used with a thallium-activated sodium iodide crystal (0.5 in.$\times$0.5 in.$\times$0.2 in.) mounted on edge in silicone grease under a polished aluminum dome on the photosensitive window. This assembly is shown in Fig. 2. The dome was sealed to the window with silicone grease and had a $\frac{1}{2}$-in. diameter hole in one side, through which the particles entered. This aperture was covered with 0.0003-in. Al foil cemented on with silicone grease. The surfaces of the crystal were thus preserved from the damaging effects of atmospheric water vapor by a silicone grease seal for the immediate crystal housing. In addition, the photomultiplier housing was filled with dry argon and sealed with $Q$-wax. Under these conditions, the resolving power of the crystal remained stable for a week or longer, indicating that the crystal surfaces did not appreciably deteriorate in that time.

The resolving power in energy is to a great extent determined by the fraction of the light pulse from the crystal which arrives at the photosensitive surface. This fraction is determined by the area of contact between the crystal and the window, the condition of the crystal surfaces, and the effectiveness of the reflecting surface. Because of limitations in space available in the scattering chamber, the photomultiplier had to be mounted vertically. To reduce background, the crystal thickness in the direction of passage of the particles was just greater than the maximum proton range (about 0.2 in.). Its face was $\frac{1}{2}$ in. square to simplify alignment with the $\frac{1}{4}$-in. aperture and the target. It was necessary to set the crystal on edge and this probably seriously affected the resolving power, which was not as good as that reported for protons by Franzen, Peelle, and Sherr.[1]

The sodium iodide was cleaved under Nujol and mounted on the photomultiplier without removing the oil film. There were 17.6 mg/cm$^2$ (Al equivalent) of material interposed between the scattering foil and the crystal consisting of the Al foil vacuum window, the Al foil crystal housing window, and the argon in the path from the vacuum window to the crystal.

## D. Pulse-Height Discrimination

The photomultiplier was operated with about 600 volts, total, across it or 60 volts per stage. Under these conditions, a 30-Mev proton produced a pulse of about one volt out of the cathode follower. These pulses were fed through a delay line clipping circuit into a Los Alamos model 501 amplifier. The pulse produced had a rise time of about 0.5 microsecond and a base width of about 1.5 microseconds followed by a small (1–2 percent) undershoot lasting about 50 microseconds.

It was found convenient to adjust the counting rate for the major part of a spectrum to about 15 counts per second or 1 count per beam pulse. With the 150 microsecond duration beam pulse, the pile-up of large pulses was negligible, and the γ-ray and neutron background pulses may have contributed through pile-up a small amount to the spread of peaks in the spectrum.

The output of the amplifier was fed both to a 10-channel pulse-height discriminator and to one vertical plate of a Tektronix model 411 AD synchroscope, with a blue screen for photography.

The 10-channel discriminator was very useful for exploration and monitoring but when used with a 2-volt channel width introduced uncertainties which reduced its value for taking a full spectrum. There were unreproducible variations in channel width as well as shifts in the location on the voltage scale of the whole set of channels, introducing errors somewhat greater than the statistical error. With a resolving power such that the full width at half-maximum of the elastic peak was about 5 percent, it was necessary to use channel widths of about 2 percent of the elastic pulse height (2 v in ~100 v). As a result, a minimum of 5 runs was required for one spectrum at one angle.

As an alternative method for taking pulse-height distributions, the vertical pulses on the synchroscope screen were photographed on a continuously-moving horizontal 35-mm film strip. In order to make economical use of the film without increasing greatly the chance of one pulse masking another, a slow horizontal sweep was used, triggered from the linear accelerator circuits. A trigger pulse was available which occurred about 500 microseconds before the beam pulse. At this time a horizontal sweep was started from the left at a rate of about 150 microseconds/cm. The pulses then occurred over a 1-cm region at the center of the screen. The screen was masked except for this central region to avoid over-exposure of the base line. In addition, a small piece of yellow plastic filter was cemented over the base line in the central region. The film was moved continuously at 1-in. per second and under these conditions, each interval corresponding to a beam pulse was recorded on the film as a region about $\frac{1}{16}$ in. long without overlap. A particle pulse appears as a faint vertical line with a dark spot corresponding to the 0.5 microsecond duration flat top. This is convenient for analysis of the film since the center of this dark spot can be used to estimate the pulse height.

With a counting rate for the major part of the spectrum of 15 counts per second, a spectrum consisting of 20,000 counts can be recorded in 20 minutes on a 100-foot film strip.
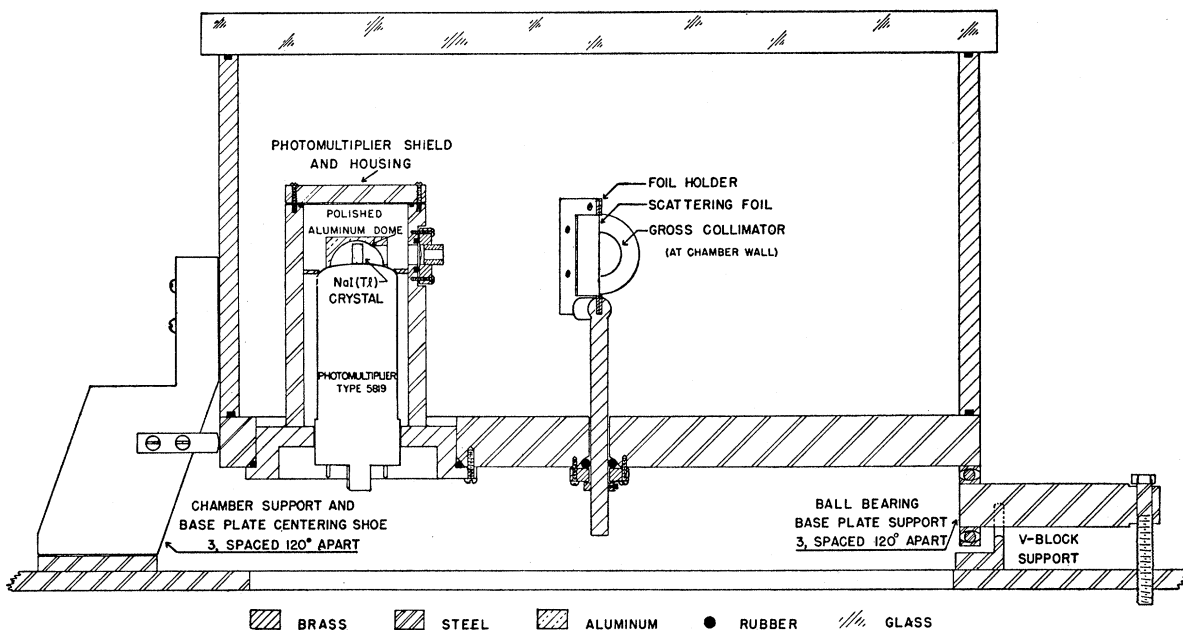


BRASS   STEEL   ALUMINUM   ● RUBBER   GLASS

FIG. 2. Cross section of scattering chamber at 90° to beam direction. The chamber is set for observation at 90° to the beam direction.

## E. Method of Film Analysis

After consideration of various methods for automatic analysis of the films using multichannel phototube circuits, etc., it was decided that the investment of development time would be prohibitive if good precision were to be obtained and counts from dirt and scratches eliminated. On the other hand, a strictly manual method of analysis was inconveniently slow.

As a practical compromise, a bank of 80 electrical registers was assembled connected to a row of 80 small microswitches. The microswitches were mounted directly on the face of a large ground glass screen in a horizontal row. An image of the film was projected onto the screen with the base line vertical, so that the pulses extended along the row of switches. As the film moved, the ends of the pulses passed individual switches which were then depressed manually. With this arrangement an increase in speed of analysis of a factor of five or ten was obtained over any strictly manual method of recording pulse heights from the film strip.

## F. The Integrator

All bombardment current integrations were made with the integrator constructed by Lee Aamodt several years ago. This integrator has been used in a number of investigations with the linear accelerator[3,4] and has given good, consistent results. It is unlikely that any significant error in the absolute cross sections has been introduced from this source.

## G. The Energy Scale

In all of this work it has been assumed that the pulse height from the photomultiplier is proportional to the energy of the particle (proton or deuteron) striking the sodium iodide crystal. The beam energy was estimated by measuring the range in aluminum. With a proper correction for recoil, the elastically scattered group of protons was then used as a calibration point for the energy scale.

The semi-empirical range-energy relation of Smith[5] was used. An approximate check on the range-energy relation is available at 32 Mev from the data of Panofsky and Phillips.[4] In this work, the energy of the beam from the linear accelerator was inferred from the frequency and drift tube dimensions to be $32\pm0.1$ Mev. The threshold of the $B^{11}(p, n)C^{11}$ reaction was measured as $3.0\pm0.6$ Mev by using absorbers to reduce the beam energy. This value checks within error with the results of Van de Graaf work. At the time of this work, the linear accelerator was not sufficiently reproducible in its behavior to allow such a precise inference as to the energy output. Another check on the range-energy

[3] Levinthal, Martinelli, and Silverman, Phys. Rev. **78**, 199 (1950).
[4] W. K. H. Panofsky and R. Phillips, Phys. Rev. **74**, 1732 (1948).
[5] J. H. Smith, Phys. Rev. **71**, 32 (1947).

relation at 18 Mev is available from the work of Hubbard and MacKenzie,[6] using a 180° deflection method inside the cyclotron at the University of California, Los Angeles.

The most precise check on the linearity of the crystal is the comparison of the $Q$ values for various excited states from this work with previously obtained values. Another good check is the energy estimated for the deuteron group from the $C^{12}(p, d)C^{11}$ reaction (see Fig. 4), where an error of 0.3 Mev is indicated.

An attempt to check the linearity of the crystal was made using aluminum absorbers to reduce the beam energy. The results of this method are not entirely satisfactory since the original beam energy spread of greater than 0.6 Mev (full width half-maximum) is increased greatly as the energy is reduced. The results are good to about $\pm3$ percent from 12 Mev to 32 Mev and are consistent with proportionality between pulse height and proton energy.

The shape of peaks in the pulse-height distribution in general appears to be symmetrical except for a slight distortion toward low energies at the foot of large peaks. The following criterion for the location of a peak on the pulse height or energy scale has been chosen: A smooth curve is drawn through the points on the peak, and a point halfway between the sides of the peak, about $\frac{3}{4}$ of the way up, has been taken as the location of the peak. Since there is an energy spread of about 0.6 Mev (full width at half-maximum) in the proton beam from the linear accelerator, the measurement of the beam energy by measuring the extrapolated range will introduce an error as far as the mean energy of the beam is concerned. As a result, 0.3 Mev has been subtracted from the value of beam energy obtained by extrapolated range measurement.

## H. Reduction of Data

A pulse-height distribution recorded on film or with 10-channel discriminator gives directly the number of particles per interval of pulse height for a known charge of bombarding protons. The bombarded nucleus, target thickness, and solid angle of the counter are known, and proportionality between pulse height and energy is assumed. Therefore, the differential cross section at a particular angle for any interval of energy referred to the center of mass system may be calculated, if the outgoing particle can be identified.

In the calculations for Figs. 4 and 7, where the center of mass differential cross section is plotted against the $Q$ of the reaction, inelastic scattering has been assumed, i.e., the outgoing particle is taken to be a proton. If the outgoing particle actually turns out to be different from a proton, small errors in cross section (less than 10 percent for laboratory energies greater than 8 Mev) appear, along with shifts of several Mev in calculated

[6] E. L. Hubbard and K. R. MacKenzie, Phys. Rev. **85**, 107 (1952).

$Q$ value. Some examples of the shifts appear on Figs. 4 and 7 and will be discussed later.

The first step in the reduction is to obtain the relationship between pulse height and laboratory energy for the particular run. The peak in the pulse-height distribution due to elastic scattering from the target nucleus is identified. The energy of the elastically scattered protons is calculated from the usual recoil formula, and a correction is made for the loss in the (17 mg/cm² Al equivalent) material interposed between the target and crystal to obtain the energy actually lost in the crystal. This energy value is used to calibrate the crystal for the particular run and by again applying the appropriate correction for the energy lost in the "window," the laboratory energy corresponding to any pulse height may be calculated.

If the outgoing particle is assumed to be a proton, then, by using the usual recoil formula, the reaction energy change $Q$ can be calculated for any given pulse height. Actually the $Q$ value was calculated for several points over the range of interest and the remainder of the values were obtained graphically. It was found that from a laboratory energy of 8 Mev up to the maximum, a linear relationship holds between $Q$ and the pulse height to better than 0.1 Mev, for beryllium and carbon.

The next step in the reduction is to calculate the center-of-mass differential cross section corresponding to each point in the pulse-height distribution. The number of particles counted in a particular interval of $Q$ is

$$n = n_0 N \frac{d^2\sigma}{d\omega dQ} \Delta Q \Delta \omega \frac{\sigma(\theta)}{\sigma(\eta)},$$

where $n_0$ is the number of bombarding protons, $N$ the scattering nuclei per cm² of target, $d^2\sigma/d\omega dQ$ the center-of-mass differential cross section in cm² steradian⁻¹ Mev⁻¹, $\Delta\omega$ the solid angle of the counter in the laboratory system, $\eta$ the center-of-mass scattering angle, and $\theta$ the laboratory scattering angle. This expression is accurate in general if the resolution width for energy is small compared with $\Delta Q$, or if $d^2\sigma/d\omega dQ$ does not change significantly within the resolution width. Since neither of these conditions is met in general in this work, the value of $d^2\sigma/d\omega dQ$ calculated will be strongly modified by the resolution width. Sharp peaks will be reduced in height and smeared out. Nevertheless, the calculated $d^2\sigma/d\omega dQ$ is useful since the resolution width is independent of $\theta$ to our accuracy and a comparison of the variation of cross section with $Q$ can be made between different angles. In addition, if correction is made for overlapping of peaks, the area under any given peak is the corresponding differential cross section in millibarns per steradian.

If $P$ is the pulse height, $\Delta Q = \Delta P dQ/dP$. $dQ/dP$ can be easily evaluated from the slope of the graph of $Q$ against $P$ for each run. $\sigma(\theta)/\sigma(\eta)$ is evaluated from the usual recoil formulas and is a minor correction amounting to a maximum of 16 percent in this work.

## III. RESULTS

### A. Carbon

A 2-mg/cm² polystyrene foil was used as a target for the work on carbon. Since the spectra were taken at angles of 90° or greater, there was no interference from the hydrogen content of the foil.

Several spectra were taken using the 10-channel discriminator and spectra at 90° and 160° were recorded on film. Since there are no inconsistencies between the 10-channel data and the film data and the accuracy and background of the film data are better, only the film data are included.

In Fig. 3 are given the actual pulse-height distributions as read from the films, less background. In Fig. 4 the calculated center-of-mass differential cross section in $10^{-27}$ cm²/steradian Mev is plotted against the calculated $Q$ value, assuming inelastic scattering. The probable errors shown are just those due to statistics. In addition, there is about $\pm 15$ percent error in absolute cross section, and a smaller relative error between the data at the two angles.

Referring to Fig. 3, the peaks occurring at greatest pulse height have been taken as due to elastic scattering. Note the peak at 52 on the 90° curve (marked $K$) which is probably due to elastic scattering from a heavy impurity in the target. The peaks due to elastic scattering from carbon have been plotted at $Q=0$ on Fig. 4 (marked $A$). The peaks marked ($B$) and ($D$) can be identified as due to inelastic scattering leading to the excitation of known levels in $C^{12}$. Table I gives the $Q$ values and cross sections measured in this work.

The excitation of the 7.4-Mev level (peak $C$) has not been previously observed in the inelastic scattering process. An analysis of the various experiments in which this level has been observed indicates that its existence is uncertain. The groups identified with the 7.4-Mev level in this work occur with such small cross section as to make the identification doubtful.

The broad peak ($E$) can, with reasonable certainty, also be identified as due to inelastic scattering from $C^{12}$. Because of the large negative $Q$ values for all competing reactions, the broad peak ($E$) cannot be due to any particles but protons resulting from $C^{12}+p$, although a contribution may be present from various particles resulting from reactions in $C^{13}$ and impurities. The $Q$ values for reactions competing with inelastic scattering, calculated from mass tables, are as follows: $(p-d)$, $-16.3$; $(p-p, n)$, $-18.7$; $(p-\alpha)$, $-7.5$; $(p-\text{He}^3)$, $-19.6$; $(p-p, 2n)$, $-32.7$; $(p-\text{H}^3)$, $-24.1$; $(p-n)$, $-18.5$; $(p-3\text{He}^4, p)$, $-7.3$. The calculated location of the peak on the 90° curve due to alpha-particles from the reaction $C^{12}(p, \alpha)B^9$ to the ground state is shown on Fig. 4 ($H'$). Although this $Q$ is only $-7.5$ Mev, the combination of recoil and energy loss in the window reduces the energy of this group of alpha-particles to about 7 Mev, at the time they strike the crystal.

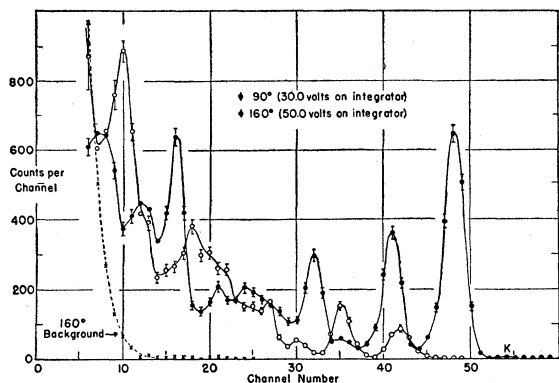$C^{13}$ is present in the target (1.1 percent) and other

FIG. 3. Pulse-height distributions, recordéd on film, for the scattering of 31.5-Mev protons from a polystyrene target. Background has been subtracted. The background for the run at 160° is included as an example.

impurities may be present in smaller quantities. However, no reaction has been suggested which, with reasonable cross section, could give the peak $(E)$. This broad peak may be due either to the excitation of broad levels or to the excitation of closely spaced sharp levels. A better resolving power is apparently necessary to show which is the case. Some evidence for levels in this region has been obtained in other reactions.[7]

The peaks $(B)$ and $(D)$ show a strong anisotropy. The ratio of the 90° cross section to the 160° cross section is about five to one. However, for the peaks $(C)$ and $(E)$ no anisotropy is indicated. This may indicate that so many levels contribute to the peak $(E)$, that the individual angular distributions are washed out, or that the levels concerned give roughly isotropic angular distributions.

The spectrum at 90° may be compared with the results of Levinthal, Martinelli, and Silverman[3] obtained as range distributions using nuclear emulsions
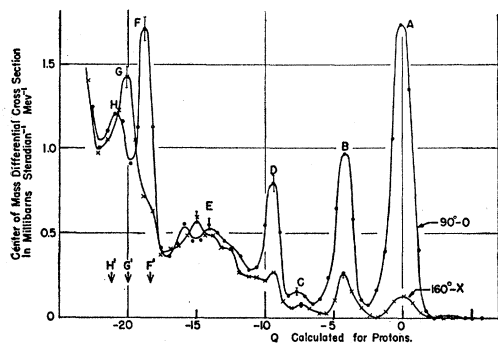


FIG. 4. $C^{12}$ center-of-mass differential cross section, calculated from the pulse-height distributions in Fig. 3, plotted against calculated $Q$ in Mev, assuming inelastic scattering.

[7] E. Stuhlinger, Z. Physik 114, 185 (1939); V. R. Johnson, Phys. Rev. 81, 316 (1951); Fowler, Gaerttner, and Lauritsen, Phys. Rev. 53, 628 (1938); A. H. Morrish, Phys. Rev. 76, 1651 (1949); R. Tangen, Kgl. Norske Videnskab. Selskabs Skrifter, No. 1 (1946); McLean, Ellett, and Jacobs, Phys. Rev. 57, 1083 (1940).

in bombarding carbon with protons of about the same energy. Levinthal et al. do not give absolute cross section figures, but the relative height and locations of the peaks $(B)$ and $(D)$ check well, and in addition, there is evidence in their data for the group $(E)$.

The peaks $(F)$ and $(G)$ are due to deuterons from the reaction $C^{12}(p, d)C^{11}$. The range distribution of Levinthal et al. shows a peak with the proper range, if it is assumed to be deuterons from a reaction ending in the ground state of $C^{11}$. The energy distributions in Fig. 3 show a peak at both 90° and 160° which has the proper energy under the same assumption.

Since the peaks $(F)$ and $(G)$ are due to deuterons, they will not fall at the proper $Q$ values on Fig. 4, where the $Q$ was calculated assuming the the outgoing particle was a proton. The arrows marked $(F')$ and $(G')$ on Fig. 4 are located at the expected positions on the 90° and 160° curves, respectively, of the deuteron peaks, assuming $Q = -16.5$ Mev, calculated from the masses given in Bethe.[8]

TABLE I. $C^{12}$ $Q$ values and differential cross sections.

| Group | Differential cross section (millibarns/steradian) | |
|---|---|---|
| | 90° | 160° |
| Elastic | 3.0 ±0.4 | 0.29±0.05 |
| Resolved inelastic, centered at: | | |
| $Q = -4.3±0.2$ Mev | 1.5 ±0.2 | 0.34±0.05 |
| $Q = -7.5±0.4$ Mev | 0.16±0.1 | 0.12±0.06 |
| $Q = -9.5±0.2$ Mev | 0.90±0.2 | 0.19±0.1 |
| Unresolved inelastic between $Q = -11$ and $Q = -17$ Mev | 2.8 ±0.4 | 2.7 ±0.4 |
| Deuteron | 1.3 ±0.6 | 1.1 ±0.6 |

The differential cross sections for the $C^{12}(p, d)C^{11}$ reaction at 90° and 160° are 1.3 and $1.1 \times 10^{-27}$ cm²/ steradian. These are lower limit figures, obtained from the areas of the peaks on Fig. 3, above smooth curves drawn to represent background from other reactions. The error is probably not greater than 50 percent. If isotropy is assumed, the total cross section becomes 15 millibarns. This figure can be compared with the total cross section for the production of $C^{11}$ of 75 millibarns measured by Panofsky and Phillips,[4] using 32-Mev protons. Thus, as a lower limit, 10–20 percent of the production of $C^{11}$ is by the $(p, d)$ reaction. It is possible that the figure should be very much higher than this, since a forward peak in the angular distribution may occur. Such a peak would be expected to occur if the reaction were considered as a pick-up process. Harvey[9] has measured the angular distribution of the ground-state deuterons in the $Be^9(p, d)Be^8$ reaction with bombarding energies from 5 to 8 Mev and observed a very strong forward peak. The intensity at 20° was 15

[8] H. A. Bethe, Elementary Nuclear Theory (John Wiley and Sons, Inc., New York, 1947).
[9] J. A. Harvey, Phys. Rev. 82, 298 (1951).

times that at 70° and the distribution was roughly isotropic at larger angles.

It is conceivable that the production of C[11] with 32-Mev protons on C[12] may be predominantly by the $(p, d)$ reaction.

## B. Beryllium

A 4.8 mg/cm^{2} rolled metallic foil of beryllium was used as a target, and charged particle spectra were obtained at 90°, 125°, and 160°. The 90° and 125° spectra shown in Fig. 5 were recorded on film and the 160° spectrum shown in Fig. 6 was recorded with the 10-channel analyzer.

Small peaks which have been identified as due to elastic scattering from impurities in the target occur at large pulse height on Fig. 6. The peak with a pulse height of 94.5 on Fig. 6 is due to elastic scattering from
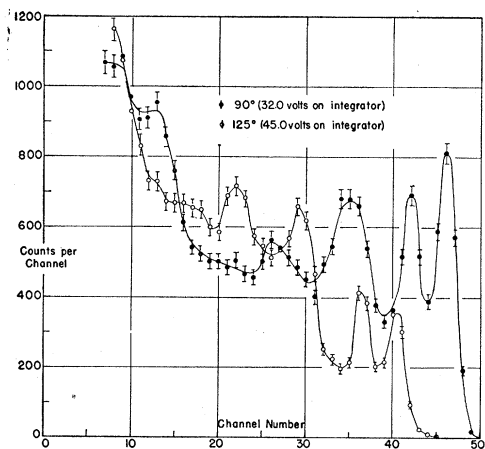
FIG. 6. Pulse-height distribution, recorded with the 10-channel discriminator for the scattering of 31.5-Mev protons at 160° from a beryllium foil target. Background has been subtracted.

FIG. 5. Pulse-height distributions, recorded on film, for the scattering of 31.5-Mev protons at 90° and 125° from a beryllium foil target. Background has been subtracted.

Be[9] and is used to calibrate the energy scale for the 160° data. The peaks with pulse heights of 46.0 and 40.5 on Fig. 5 are due to elastic scattering from Be[9] at 90° and 125°, respectively, and are used to calibrate the energy scales for the data at these angles.

On Fig. 7 the calculated center-of-mass differential cross section is plotted against the calculated $Q$, assuming inelastic scattering from Be[9], for the spectra at the three angles.

Some of the groups appearing in these spectra can be identified as due to inelastic scattering leading to the excitation of previously unobserved levels in Be[9]. As a result, it is important to rule out the possibility of impurities in the target having a strong influence on the spectra. An analysis of a sample of beryllium foil from the same lot as the target indicated the following impurities: Al, 0.1–1 percent; Ca, Mg, 0.01–0.1 percent; Cr, Fe, <0.01–0.1 percent. In addition, there was a barely visible layer of oxide on the surface of the foil.
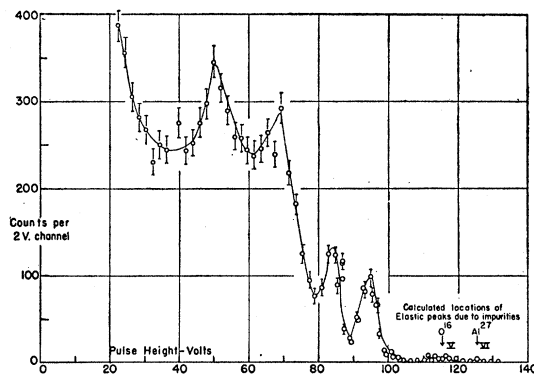
On Fig. 6 the calculated locations of elastic peaks due to O[16] and Al[27] are plotted, assuming the peak at 94.5 is due to elastic scattering from Be[9]. The peaks occurring in this region of pulse height are apparently due to impurities of about the mass of oxygen and aluminum. Since these are the principal expected impurities, for the purpose of estimating the effect on the remainder of the spectrum, we can assume that these are the only significant impurities.

Taking the peak marked *VI* to be due to aluminum, and using the values of the cross sections for elastic scattering listed in Table IV, the amount of aluminum impurity is estimated to be $2\pm1$ percent by weight. It can be seen by referring to the 160° aluminum spectrum, Fig. 9, that this amount of aluminum will have an entirely negligible effect on the spectrum. The peak presumably due to oxygen is somewhat greater, amounting to about 5 percent of the beryllium elastic peak.

The spectrum caused by oxygen is unknown. However, any peaks in the beryllium spectrum that were due to oxygen would exhibit a shift with angle on Fig. 7, where the differential cross section is plotted against $Q$ calculated for inelastic scattering of protons from Be[9]. As an example of this shift, the calculated positions
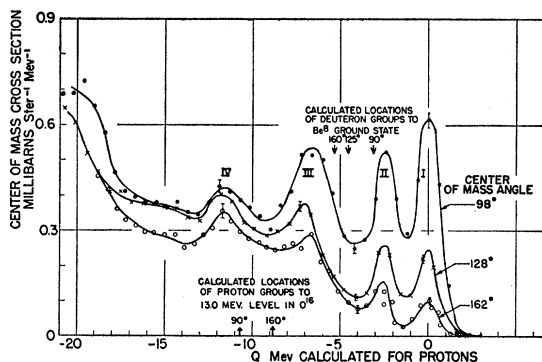
FIG. 7. Be[9] center-of-mass differential cross section calculated from the pulse-height distributions in Figs. 5 and 6, plotted against calculated $Q$ in Mev, assuming inelastic scattering.

TABLE II. $Q$ values calculated from film and 10-channel data, assuming inelastic scattering or the reaction $Be^9(p, d)Be^8$.

| Excited state, Mev | Laboratory angle | $Q$, Inelastic scattering | | $Q$, $Be^9(p, d)Be^8$ 10-channel data Mev |
|---|---|---|---|---|
| | | Film data Mev | 10-channel data Mev | |
| 2.5 | 90° | −2.45 | −2.49 | +1.34 |
| | 125° | −2.50 | −2.41 | +3.11 |
| | 160° | | −2.70 | +3.49 |
| 6.8 | 90° | −6.7 | −6.61 | −3.26 |
| | 125° | −7.1 | −6.85 | −2.15 |
| | 160° | | −6.72 | −1.06 |
| 11.6 | 90° | −11.5 | −11.43 | −8.68 |
| | 125° | −11.8 | −11.48 | −7.45 |
| | 160° | | −11.55 | −6.82 |

of peaks due to inelastic scattering from $O^{16}$ leading to excitation of a 13.0-Mev level are plotted. The shift from 90° to 160° for this case is 1.8 Mev, and the amount of this shift does not change strongly with energy, being 2.0 Mev at $Q=0$ and about 1.6 Mev at $Q=-18$.

It cannot be said with certainty to what extent the spectra are made up of protons, deuterons, or other particles. However, with considerable certainty the peaks marked II, III, and IV on Fig. 7 can be identified as due to protons. Table II lists the $Q$ values corresponding to the center of these peaks, assuming that they are due either to protons or deuterons. These values were calculated from the pulse-height distributions shown in Figs. 5 and 6 and from two additional 10-channel distributions which are not reproduced.

The values in column 5 vary between 90° and 160° by 2 Mev or more, which is clearly outside error. The values in column 3, however, vary by less than 0.3 Mev which is the order of precision to be expected in locating fairly broad and occasionally unsymmetrical peaks. If these peaks can be identified with each other as they have been in Table II, they are due to protons. No alternative identification has been successful.

If a reaction were to lead to a discrete group of particles heavier than deuterons, say $He^3$ or $He^4$, the apparent shift in $Q$ with angle on Fig. 7 would be considerably larger than that shown for the deuterons to the ground state of $Be^8$.

It can be concluded, then, that states, or closely-spaced groups of states, in $Be^9$ at 2.5, 6.8, and 11.6 Mev have been excited in the inelastic scattering process. The first of these states is presumably identical with the 2.41-Mev level observed by Davis and Hafner[10]

TABLE III. $Be^9$ excitation energies and cross sections.

| Excited state Mev | Differential cross section (millibarns/steradian) | | |
|---|---|---|---|
| | 90° | 125° | 160° |
| 2.5±0.2 | 0.64±0.3 | 0.34±0.1 | 0.18±0.05 |
| 6.8±0.3 | 0.6 | 0.2 | 0.1₄ |
| 11.6±0.4 | 0.1₇ | 0.1₃ | 0.2₁ |

[10] K. E. Davis and E. M. Hafner, Phys. Rev. 73, 1473 (1948).

from the inelastic scattering of protons up to 7.1 Mev, and by Rhoderick,[11] also from the inelastic scattering of protons. The 6.8- and 11.6-Mev states have not been observed previously in any reaction. However, there do not appear to be any reports in the literature of experiments in which the observation of these states could be expected.

In Table III are listed the average values for the energies of the excited states and the approximate differential cross sections at three angles.

The principal source of error in the evaluation of these cross sections is the continuous background in the pulse-height distribution due to particles from other reactions. In order to estimate the cross sections for the 6.8- and 11.6-Mev levels, a smooth curve representing the background has been drawn through the valleys between the peaks. The figures listed in Table III are based on the area under the peaks above this curve and therefore are lower limits for the cross sections. It is is difficult to estimate the accuracy of these figures. The figures for the 2.4-Mev level are based on the area

TABLE IV. Measured differential cross sections for the elastic scattering of 31.5-Mev protons.

| Element | Lab angle | c.m. angle | c.m. cross section (millibarns steradian⁻¹) | Ratio 90°/160° |
|---|---|---|---|---|
| $Be^9$ | 160 | 162.4 | 0.19±0.04 | 7±1 |
| | 125 | 127.5 | 0.32±0.05 | |
| | 90 | 97.9 | 1.3 ±0.3 | |
| $C^{12}$ | 160 | 161.7 | 0.29±0.05 | 10±1 |
| | 90 | 95.6 | 3.0 ±0.4 | |
| $Al^{27}$ | 160 | 160.7 | 0.59±0.1 | 6±2 |
| | 90 | 92.3 | 3.5 ±0.5 | |
| Pb | 155 | 155 | 0.79±0.2 | 9±3 |
| | 90 | 90.1 | 6.8 ±2 | |

above the baseline of symmetrical peaks, allowing for some overlapping.

### C. Aluminum

The target for the aluminum bombardments was a 3.36 mg/cm² sample of commercial pure aluminum foil.

On Fig. 8 are shown the pulse-height distributions taken with the 10-channel discriminator. On Fig. 9 is shown the differential cross section in millibarns steradian⁻¹ Mev⁻¹ as a function of the laboratory energy of the outgoing particles. Figure 9 is given as a semilog plot in order to show the approximately exponential shape of the spectra, which is similar to the results of Gugelot[12] and others on neutron spectra.

Included for comparison purposes on Fig. 9 is a dotted curve representing the results of Levinthal, Martinelli, and Silverman.[3] This curve is a transformation to proper scales of a smooth curve drawn through their experimental points. Their results were obtained

[11] E. H. Rhoderick, Proc. Roy. Soc. (London) A201, 348 (1950).
[12] P. C. Gugelot, Phys. Rev. 81, 51 (1951); P. H. Stelson and C. Goodman, Phys. Rev. 82, 69 (1951).

as range distributions using nuclear emulsions, at an angle of 96° with 30.4 Mev bombarding protons. The vertical dotted bars represent their quoted probable errors, which are just those due to statistics. The errors shown on the 90° and 160° curves are also just those due to statistics.

Levinthal *et al.* quote 4.1 millibarns steradian$^{-1}$ as the differential cross section for elastic scattering at 96°. The result from this work, appearing in Table IV, is 3.5±0.5 millibarns steradian$^{-1}$.

### D. Platinum and Lead

Spectra taken with the 10-channel discriminator at 90° for platinum and lead are shown in Fig. 10. A number of other runs were taken with broad channels and all check the shape of the spectra within statistical error. These data were taken in the earlier stages of the work before the background and resolution had been improved to the degree later obtained. Also included on Fig. 10 is the peak for elastic scattering taken at 25° from the same target immediately after the 90° lead spectrum was taken. The 90° lead elastic peak has been spread, possibly due to the excitation of low-lying levels.

### IV. ELASTIC SCATTERING

### A. Experimental Results

Measurements of the differential cross section for elastic scattering were obtained from each of the spectra reproduced in Sec. III. In addition, values were obtained from a number of exploratory runs using the 10-channel discriminator. Table IV gives average values of the measured differential cross sections in millibarns per steradian.

The probable errors quoted in Table IV, column 5 include ±15 percent due to various errors in measurement of target thickness, solid angle, integrated current, target angle, as well as the effect of variations in beam position on the effective solid angle. In addition, allowance has been made for counting statistics and in some cases for possible contribution of unresolved, low-lying levels to the apparent elastic peak. The ratio of the cross section at 90° to that at 160° is generally known with greater precision since some of the errors drop out.

The ratio of the differential elastic scattering cross section at 90° to that at 160° does not vary among the four elements by an amount which is significantly greater than the probable errors quoted. In addition, there is a fairly smooth increase in differential cross section with atomic weight. From the smooth behavior of the elastic scattering cross section as a function of $A$, it appears very unlikely that the experimental results are fortuitously located in sharp valleys in the angular distributions. If the spectra showed sharp peaks and valleys, the location and spacing of the peaks would be
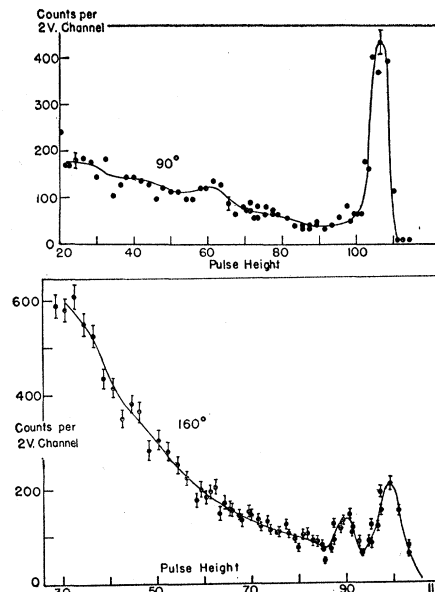


FIG. 8. Pulse-height distributions, recorded with the 10-channel discriminator for the scattering of 31.5-Mev protons from an aluminum foil target. Background has been subtracted.

expected to change radically as $kR$ changes from 5 (Be) to 14 (Pb).

### B. Discussion of Elastic Scattering

These results suggest that the constitution of the individual nuclei has a relatively minor effect on elastic scattering at this energy. As a result, it is conceivable that some simple nuclear model might be chosen which would give predictions in agreement with experimental results.
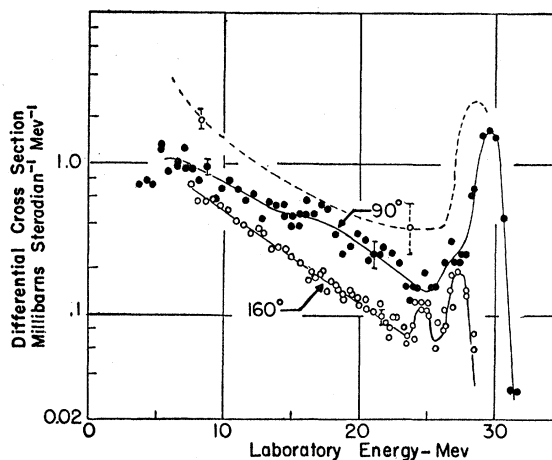


FIG. 9. Semilog plot of Al$^{27}$ center-of-mass differential cross section calculated from the pulse-height distributions in Fig. 8, assuming inelastic scattering. The broken curve represents the results of Levinthal, Martinelli, and Silverman (see reference 3) obtained as a range distribution using nuclear emulsions with a laboratory angle of 96° and 30.5 Mev bombarding energy.
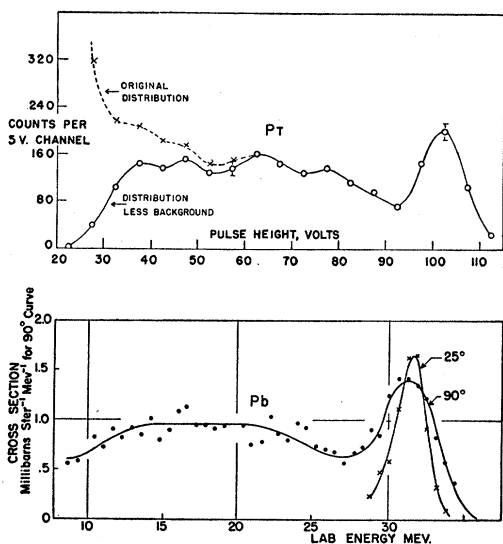
FIG. 10. Pulse-height distributions recorded with the 10-channel discriminator for the scattering of 31.5-Mev protons at 90° from lead and platinum. Background has been subtracted.

A number of models have been investigated, and agreement in order of magnitude has not been obtained. Table V summarizes the results. In addition, Fig. 11 shows the angular distributions calculated for the various models.

The total cross sections for neutron scattering and absorption are listed as well as the differential cross sections since they are fairly well known experimentally[13] and give a good control on the choice of models.

In all but one case, the differential cross sections have been calculated for neutrons, to avoid the use of Coulomb wave functions. It is reasonable to expect that the 2- or 3-Mev Coulomb barrier (beryllium) compared with a 30-Mev nuclear potential and a 32-Mev bombarding energy will have a small effect on scattering cross section at large angles. This is corroborated by the com-

TABLE V. Calculated scattering cross sections. In row 7, for comparison, are given the experimental results for beryllium. The differential cross section figures are from this work and the total cross section figures are from neutron scattering work (see references 13 and 16).

| Model | Total cross sections (barns) | | Differential cross sections (millibarns steradian$^{-1}$) | | | |
|---|---|---|---|---|---|---|
| | Scattering | Absorption | 90° | 125° | 160° | 180° |
| 1 Totally reflecting sphere | 1.4 | 0 | 53 | 40 | 48 | 32 |
| 2 Totally reflecting sphere +Coulomb field | — | 0 | 68 | 7 | 74 | 97 |
| 3 Total absorption of partial waves up to $l=4$ | 0.55 | 0.55 | 6.1 | 3 | 6.5 | 44 |
| 4 Square well | 2.3 | 0 | 24 | 14 | 33 | 193 |
| 5 Square well with absorption | 1.4 | 0.55 | 16 | 5 | 1.5 | 24 |
| 6 Adjusted phase shifts | 0.47 | 0.51 | 1.0 | 0.12 | 0.17 | 0.01 |
| 7 Experimental, beryllium | 0.5 | 0.5 | 1.3 | 0.32 | 0.19 | — |

[13] Amaldi, Bocciarelli, and Caccipuoti, Nuovo cimento **3**, 15, 203 (1946); translated in Report of Cambridge Conference on Fundamental Particles, pp. 97–113 (Phys. Soc., London, 1947).

parison of the results of calculations for neutron scattering and proton scattering from a totally reflecting sphere, with a $Z$ of 4, shown in Table V. It is apparent from this case that if a close comparison were required between calculated and experimental results for proton scattering at 32 Mev for light elements, the Coulomb field could not be neglected. However, since in these calculations the order of magnitude only is of interest, the Coulomb field has been neglected.

Discussion of the calculations[14] will be limited to a brief description of the various models. The partial wave analysis of Rayleigh[15] has been used throughout. The bombarding energy has been taken as 31.5 Mev and the nuclear radius has been chosen such that $kR=5$. This value for the nuclear radius is based on various fast neutron scattering cross section measurements for beryllium.[13,16]

### 1. The Totally Reflecting Sphere

The boundary condition for this case is just that the wave function is zero at the surface of the "nucleus." There is no field external to the "nucleus."

### 2. The Totally Reflecting Sphere+Coulomb Field

In this case, the boundary condition is again that the wave function is zero at the surface of the "nucleus." The external field is that due to a nuclear charge of 4 (beryllium). We were very fortunate in obtaining a pre-publication copy of the tables of Coulomb wave functions[17] from Dr. Gregory Breit. This table lists the necessary functions from $l=0$ to $l=4$, and values for $l=5$ to $l=7$ were obtained by extrapolation. These higher angular momenta had little effect on the scattering at large angles so that the accuracy of the extrapolation was unimportant.

### 3. Total Absorption of Partial Waves up to $l=4$

The outgoing part of each partial wave from $l=0$ to $l=4$ is set equal to zero. In turn, the absorption and phase shift for all waves with $l>4$ are set equal to zero. This case corresponds to a semiclassical picture of the nucleus in which the waves corresponding to particles with collision parameters such that they will strike the nucleus are completely absorbed and all others are unaffected. It also corresponds roughly to the optical analogy of a black disk if diffraction at the edges is

[14] A more detailed description, including tables of the phase shifts and amplitudes for the important angular momenta appears in the author's thesis (Princeton University, 1951) and in a project report, "The Scattering of 32 Mev Protons from Several Elements," June, 1951, Palmer Physical Laboratory, Princeton, New Jersey (unpublished).

[15] J. W. Rayleigh, *Theory of Sound* (Dover Publications, New York, 1945), second edition, p. 323; N. F. Mott and H. S. W. Massey, *The Theory of Atomic Collisions* (Oxford University Press, London, 1949), p. 19 ff; D. Bohm, *Quantum Mechanics* (Prentice-Hall, Inc., New York, 1951), Chap. 21, p. 557 ff.

[16] R. Sherr, Phys. Rev. **68**, 240 (1945).

[17] Bloch, Hull, Broyles, Bouricius, Freeman, and Breit, Phys. Rev. **80**, 553 (1950).

ignored.[18] This model is closely related to the picture used in the usual definition of the nuclear radius from scattering experiments, since it gives for both the total scattering and total absorption cross sections

$$\frac{\pi}{k^2} \sum_{l=0}^{kR-1} (2l+1) = \pi R^2.$$

On Fig. 11 the angular distribution for the case of total absorption from $l=0$ to $l=3$ is also given in order to judge the sensitivity to the point at which the cutoff is made.

### 4. Square Well

In this case, a square well with radius$=4.17\times10^{-13}$ cm and depth$=30$ Mev was taken to represent the nucleus. The boundary condition is that the wave function outside the well is continuous with the wave function inside. Owing to the complexity of the numerical calculation, it has not been possible to vary the parameters of the well.

### 5. Square Well with Absorption

For this model, a square well with a complex potential was used. The imaginary part of the potential was chosen to be 6 Mev, which gives a total absorption cross section about equal to the experimental value. The radius and depth of the well were the same as in case 4, above. This case is similar to the partially transparent nuclear model used by Fernbach, Serber, and Taylor[18,19] to explain the results of high energy scattering experiments. The absorption coefficient, for the wave function inside the nucleus, chosen here (corresponding to the 6 Mev imaginary part of the potential) is, however, about twice the value resulting from the adjustment to the high energy scattering results made by Fernbach et al.

The boundary condition is again that the wave function be continuous passing from inside to outside the well. The solution inside involves Bessel functions of complex argument, and since tabulations of these functions are not available, a Taylor expansion of the solution was used.

### 6. Adjusted Phase Shifts

The models described give differential cross sections at large angles a factor of 10 or so larger than the experimental values. Although not leading to any specific model, it has been possible, as a result of experience with the above calculations, to specify a set of amplitudes and phase shifts which give an order of magnitude agreement between the calculated and experimental differential cross sections. These amplitudes and phase shifts give, at the same time, about the experimental values for the total cross sections.

[18] Fernbach, Serber, and Taylor, Phys. Rev. **75**, 1352 (1949).

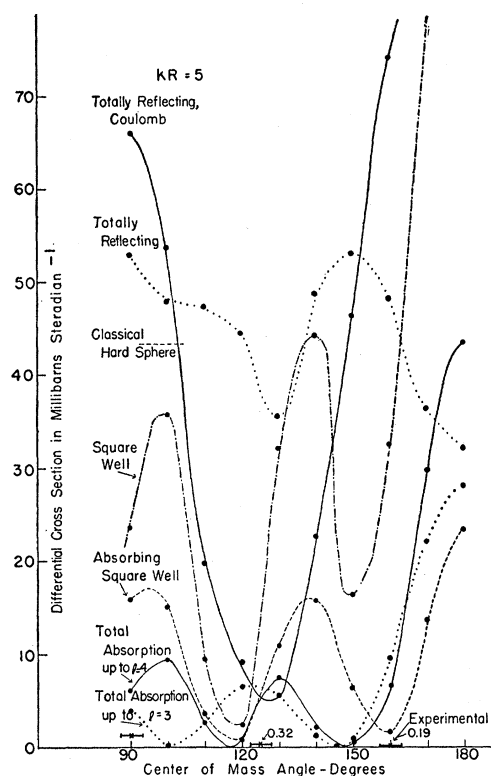[19] S. Pasternack and H. S. Snyder, Phys. Rev. **80**, 921 (1950); R. Serber, Phys. Rev. **72**, 1114 (1947).



FIG. 11. Calculated angular distributions for elastic scattering into the backward hemisphere for the various models described in the text. The three horizontal bars are the experimental points for beryllium, the length of the bar representing the 6° angular aperture of the counter.

In terms of the phase shift $\delta_l = a_l + ib_l$ the total scattering and absorption cross sections are

$$\sigma_s = \frac{\pi}{k^2} \sum_{l=0}^{\infty} (2l+1)(1+e^{-4b}-2e^{-2b}\cos 2a_l),$$

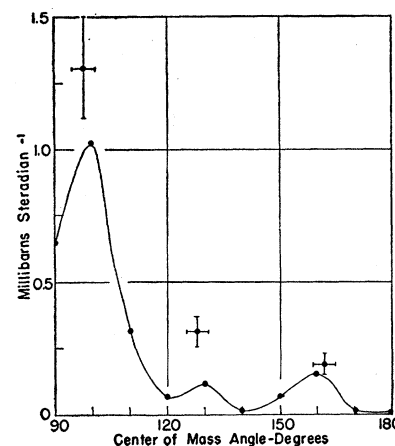$$\sigma_a = \frac{\pi}{k^2} \sum_{l=0}^{\infty} (2l+1)(1-e^{-4b}),$$



FIG. 12. Differential cross section calculated from the adjusted phase shifts, compared with the experimental values for beryllium.

and the differential cross section is

$$\frac{d\sigma}{d\omega}=\frac{1}{4k^2}\{|\sum_l(2l+1)\chi_l P_l|^2+|\sum_l(2l+1)y_l P_l|^2\},$$

where $\chi_l=e^{-2b_l}\cos2a_l-1$ and $y_l=e^{-2b_l}\sin2a_l$. In principle, within broad limits, it would be possible to solve for the phase shifts and amplitudes, given the total cross sections and differential cross sections at a sufficiently large number of angles. However, for $kR=5$ the set $a_l+ib_l$ consists of twelve numbers which have a significant effect on the angular distribution. (In none of the models investigated has there been any significant contribution to the cross sections for $l>kR$. As a matter of fact, the contributions approach zero quite rapidly in the neighborhood of $l=kR$.) In addition, the equations for $d\sigma/d\omega$ are not linear and contain both the sine and cosine of $2a_l$.

The method followed was to make an educated guess at a set of phases and amplitudes controlled by the total cross sections and, for a starting point, by the idea that if the nuclear potential were softer than a square well the phase shifts and absorption for $l=2$ and $l=6$ would be smoothly converging. Total absorption for $l=0$ and $l=1$ was assumed for convenience since this seemed reasonable and had no great influence on the result. It was possible by inspection of the resulting $d\sigma/d\omega$ to judge which $P_l(\cos\theta)$ was predominant and to make small corrections in the phase shifts. Actually, two corrections were sufficient to bring the $d\sigma/d\omega$ to the result shown in Fig. 12. Further slight corrections, of the order of 10 percent in $x_l$ and $y_l$ could be made which would reduce the average value of $d\sigma/d\omega$ in the region shown by a factor of five and have almost any desired effect on the shape of the angular distribution, without importantly influencing the total cross sections. It did not seem valuable to make further adjustments in view of the possible effect of the Coulomb field, the small number of angles for which data are available, and the limited accuracy with which the total cross sections are known.

An extreme sensitivity to the individual phase shifts of the differential cross section for backscattering results from the small value of the cross section. Almost complete cancellation has occurred in both parts of the expression for $d\sigma/d\omega$.

It appears, from this result, that fairly rough experimental results on the backscattering of neutrons could lead to accurate determination of the phases and amplitudes for the different angular momentum waves. This will be particularly true if the cross sections for backscattering are as low as would be indicated by the proton scattering results reported here. Given the phases and amplitudes, for several bombarding energies, considerable insight into the structure of a complex nucleus might be obtained.